1 Wheat Root System Architecture and Soil Moisture Distribution in an Aggregated Soil

2 using Neutron Computed Tomography.

3 Tinashe Mawodza[1*], Genoveva Burca[2], Stuart Casson[1], Manoj Menon[3]

4 [1]Department of Molecular Biology and Biotechnology, The University of Sheffield, Western

5 Bank, Sheffield S10 2TN, United Kingdom

6 [2]STFC, Rutherford Appleton Laboratory, ISIS Facility, Harwell, OX11 0QX, UK

7 [3]Department of Geography, The University of Sheffield, 9 Northumberland Rd, Sheffield S10

8 2TN

9 * Corresponding author E-mail address: tmawodza1@sheffield.ac.uk

10 Non-invasive techniques are essential to deepen our understanding of root-soil interactions in

11 situ. Neutron computed tomography (NCT) is an example of such techniques that have been

12 successfully used to study these interactions in high resolution. Many of the studies using

13 NCT however, have invariably focused on lupine plants and thus there is limited information

14 available on other more commercially important staple crop plants such as wheat and rice.

15 Also considering the high neutron sensitivity to hydrogen (e.g. water in roots or soil organic

16 matter), nearly all previous in-situ NCT studies have used a relatively homogeneous porous

17 media such as sand, low in soil organic matter and free from soil aggregates, to obtain high-

18 quality images. However to expand the scope of the use of NCT to other more commercially

19 important crops and in less homogenous soils, in this study we focused on wheat root growth

20 in a soil that contained a considerable amount of soil organic matter (SOM) and different

21 sized aggregates. As such, the main aims of this research were (1) to unravel wheat (Triticum

22 aestivum cv. Fielder) root system architecture (RSA) when grown in an aggregated sandy

23 loam soil (<4 mm) with 4% SOM content, (2) Map in 3D, soil water distribution after a brief

24 drying period and (3) to understand how the root system interacts with soil moisture

distribution brought about by soil structural heterogeneity. To achieve these, wheat seedlings

were grown for 13-days in aluminium tubes (100 mm height and 18 mm diameter) packed

with soil and imaged for the first time at the IMAT neutron beamline (in the Rutherford

Appleton Laboratory, UK). To the best of our knowledge, this is also the first study to use

NCT to study wheat root architectural development. Our study proved that NCT can

successfully be used to reveal wheat RSA in a heterogeneous aggregated soils with moderate

amounts of SOM. Lateral root growth within the soil column was increased in regions with

increased finer soil separates. NCT was also able to successfully map water distribution in a

3D and we show that large macro-aggregates preferentially retained relatively higher soil

moisture in comparison to the smaller soil separates within our samples (Fig. 1). This

highlights the importance large macro-aggregates in sustainable soil management as they

may be able to provide plants water during periodic dry spells. More in situ investigations are

required to further understand the impact of different aggregate sizes on RSA and water

uptake.
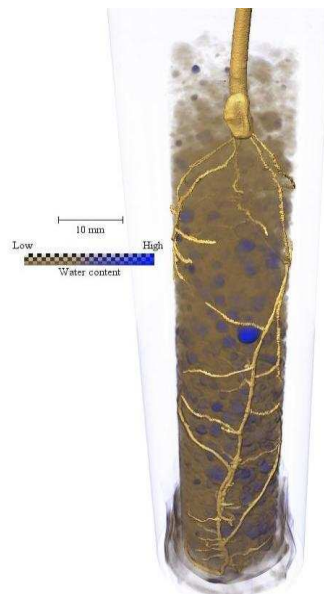
Figure 1: NCT image of a 13-day old wheat seedling root growing in an aggregated sandy
loam soil. The colour map indicates water distribution within the soil column.

Key Words: Wheat, Root architecture, Neutron Computed tomography; Water dynamics

1. **Introduction**

The seemingly insurmountable task of feeding a growing global population with increasingly limited natural resources is one of the greatest challenges facing humanity in the 21st century (Borlaug and Dowswell, 2003; Lal, 2016). With the effects of climate change threatening to further disturb global production patterns across the world, it is imperative for the research community to devise possible strategies to increase global crop productivity in the forthcoming decades (IPCC, 2007; Knox et al., 2012). This will require a deeper understanding of factors affecting crop production systems using contemporary technologies. One such area of research that has received increased attention of late is that of belowground root-soil interactions. These interactions are a vital part of the crop production system as plants acquire the majority of the resources they use for production via these associations and thus increasing our understanding of these interactions may hold the key for a 'second green revolution' required to feed a rapidly growing population (Gewin, 2010; Lynch, 2007; Rich and Watt, 2013).

Understanding root-soil interactions especially amongst the worlds' major cereal crops (maize, wheat, rice) is of paramount importance for the attainment of sustainable global food security as these crops provide more than two thirds of all human dietary energy (Cassman, 1999; FAOSTAT, 2019; Khoury et al., 2014). This understanding is crucial for wheat in particular as it is arguably the worlds' most important staple food crop. It accounts for more than 15% (220 million ha) of global arable land use, (the highest for any cultivated plant) and often yields in excess of 700 million metric tonnes of grain per annum globally (FAOSTAT, 2019). In spite of its great importance however, yield gaps in wheat production still exist, often as a result of poor adaptation of its root system to varying edaphic conditions (Senapati and Semenov, 2019; Waines and Ehdaie, 2007). As such increased research into root-soil interactions in wheat to tailor its root system for different soil environments is

69 pivotal for improving wheat yields especially in marginal areas (Alahmad et al., 2019;

70 Figueroa-Bustos et al., 2018; Waines and Ehdaie, 2007).

71 Traditionally these root-soil interactions have been investigated using either inference root

72 health from the development of above ground parts (shoots) or by the more labour intensive

73 invasive soil excavation methods (Pierret, et al. 2005). These observations however, although

74 useful, lacked critical root developmental detail required to make conclusive inferences into

75 how best to improve plant productivity (Mooney et al., 2012). Even when elements of the

76 root-soil interactions were deduced, high throughput measurements were often very difficult

77 to obtain which limited research into subterranean interactions.

78 The advent of non-invasive soil imaging in the late 70's marked a significant step forward in

79 the study of plant-soil interactions with technologies such as X-Ray Computed Tomography

80 (X-Ray CT) (Crestana, et al, 1986; Keyes et al., 2013; Tracy et al., 2013; Ahmed et al., 2016;

81 Blunk et al., 2017; Burr-Hersey et al., 2017; Koebernick et al., 2017), Magnetic Resonance

82 Imagery (MRI) (Metzner et al., 2015; Pflugfelder et al., 2017; Stingaciu et al., 2013), Nuclear

83 Magnetic Resonance imaging (NMR)(Bačić and Ratković, 1987; Brown et al., 1991;

84 Southon, et al, 1992) and Neutron imaging (NI) (Willatt, et al, 1978; Furukawa, et al. 1999;

85 Menon et al., 2007; Tötzke et al., 2017) being used to answer a multitude of questions about

86 root-soil interactions in great detail. Of these technologies NI has been the most effective

87 non-invasive soil imaging technique used when studying water dynamics and root growth

88 within the soil due to its high sensitivity to hydrogen which is abundant in water (Robinson,

89 et al. 2008). Willatt. et al, (1978), demonstrated the use of this method for the first time,

90 successfully imaging roots of different plants (soya bean and maize) growing in soil.

91 Subsequently this technology was used by in many studies including Willatt and Struss

92 (1979), Couchat et al., (1980), Bois and Couchat, (1983), (Nakanishi, et al 1992) as well as

93 Furukawa, et al. (1999). Two papers by Menon et al (2007) and Moradi et al., (2009) also

94   provided a comprehensive, accurate description of NI that subsequently led to even more

95   insightful studies using NI.

96   Initial plant experiments with NI involved the use of 2 dimensional neutron radiography (NR)

97   to study the root architectural properties in situ (Bois and Couchat, 1983; Couchat et al.,

98   1980; Willatt and Struss, 1979) using thin slabs made of aluminium. The most extensively

99   used plants in NI have been maize (Zea mays L.) pioneered in experiments by Willatt, et al.

100   (1978) and lupine (Lupinus albus L.) first used by Nakanishi, et al. (1992) with the majority

101   of papers being published on NI in plant-soil interaction mainly focusing on them. Research

102   in soil NI has since moved on to the study of more complex root-soil processes such as

103   dynamics of water flux and the extent of rhizosphere which had previously been difficult to

104   study using other techniques (Carminati et al., 2010; Oswald et al., 2008). Visualisation of

105   water movement coupled with the ability to use tracers such as heavy water (D_2O) in NI has

106   led to a better understanding of water uptake and transport in specific roots with

107   Zarebanadkouki, et al. (2013) showing that most of the water uptake in 3 week old lupine

108   plants is carried out by the lateral roots with the tap root mainly acting as a conduit for

109   upwards water movement.

110   Unlike NR, there have been fewer studies that have used neutron computed tomography

111   (NCT) to study soil-root water dynamics despite the fact that computed tomography has the

112   potential to provide even more detailed 3D visualisation of plant-soil systems as compared to

113   NR. Its uptake may have been limited by the size of the specimen that can be successfully

114   imaged in detail (usually no more than 20mm in diameter) as well as the time required for

115   such images to be taken, which is much longer than that for individual neutron radiographs

116   (Warren et al., 2013). The initial work done by Tumlinson et al., (2008) and Esser et al.,

117   (2010) with maize seedlings and lupine seedlings showed that visualisation of root and water

118   distribution dynamics in soils can be visualised successfully in 3D using NCT with improved

root-soil contrast as compared to other non-invasive imaging techniques. Moradi et al., (2011) went a step further in their study with lupine plants showing that water dynamics at the microscale can be accurately observed in 3D and thus can be used in complex and precise modelling operations explaining rhizosphere water flux. Recent advancement in NCT by Zarebanadkouki et al., (2015) who visualised 3D water dynamics of lupine plants in real time, provide great prospects of the use of NCT in further plant-soil interaction studies.

Regardless of the recent advancements in NCT in plant-soil interaction studies, there are some important limitations for this technique. For example, all of the previous studies utilising NCT have used soils containing no less than 90% sand, which are mostly devoid of organic matter or macro-aggregates. Therefore, for a wider application of this method it will require testing further using a variety of soil textures and structures. Also conspicuous in many NI studies to date is the absence wheat root architectural investigations using this technology despite the crop being major contributor to global food security. As such it is important to test the feasibility of the use of NI on wheat plants, with the aim of enhancing knowledge on wheat roots and their interactions with soil moisture.

In this paper, we thus aimed at determining the 3D root architecture of wheat seedlings grown in an aggregated sandy loam soil with 4% organic matter content using NCT. Our specific objectives were to use NCT to: a) Map 3D wheat root architectural distribution within an aggregated sandy loam soil b) Visualise in 3D, soil water distribution after a brief drying period and (c) to understand how the root system architecture interacts with soil moisture distribution as brought about by soil structural heterogeneity within an aggregated soil.

2. Materials and methods

2.1 Sample preparation and plant growth

The soil used in this experiment was a sandy loam soil (70% Sand, 17% Clay, and 13% Silt) obtained from Cove farm (53°30'03.7"N 0°53'57.2"W) and had an organic carbon content of 5.59%. This soil was air dried and mechanically sieved through a 4mm sieve to eliminate large clods and aggregates. The sieving produced a dry aggregate size distribution of 24% for particles <250µm, 36% for 250-500µm, 13% for 500-1000 µm, 13% for 1000-2000µm and 14% for 2000-4000µm with 4% SOM. This was then packed into specially designed, closed bottom, cylindrical aluminium tubes (18mm internal diameter $\times$ 100mm height) to ensure a bulk density of 1.2g cm^{-3} within the tubes. A single wheat (Triticum Aestivum. L cv. Fielder) seed was sown about 1cm underneath the surface of the soil and the tubes were watered to a volumetric moisture content (θ) of 16.0±3.0% which was experimentally determined (using gravimetric methods) to be the field capacity of our growth tubes. This water content was maintained during the course of this experiment by daily surface irrigation to the predetermined weight corresponding to the above mentioned θ for each tube. The wheat seedlings were grown for 13 days (starting from date of planting) in a growth chamber maintained at a temperature of 22°C (day)/18°C (night) and a relative humidity of 55% with light intensity averaging 400µmol m^2 s^{-1} with an 8-hour day length. Watering was stopped 4 days before neutron imaging was carried out to enhance the contrast between the root and soil.

2.2 Neutron computed tomography set up

Neutron CT imaging was carried out at the IMAT neutron imaging beamline of the ISIS Neutron and Muon Source at the Rutherford Appleton Laboratory, UK. A more detailed description of the IMAT imaging station can be found in (Burca et al., 2013); Kockelmann et

167   al., 2013 and Burca et al., 2018). For these experiments the neutron beam was shaped to the

168   field of view of 112.7 mm × 112.7 mm accompanied by a multiaxial tomography stage

169   allowing for 2 simultaneous scans. The neutron radiographies were acquired with an optical

170   camera box equipped with Andor Zyla 4.2 PLUS sCMOS with 2048×2048 pixels, an 85mm

171   lens and 100 µm 6LiF/ZnS: Ag scintillator. The images produced had a pixel and voxel size

172   of 55µm with 30s being the exposure time for each projection and an L(10000mm) /D

173   (40mm)= 250. The time taken for a single scan of the plants was almost 6 hours with 654

174   radiographs being recorded using a rotation step of 0.55°. This was the best set up achievable

175   on IMAT, suitable for our experiment (Mawodza et al., 2018).

176   2.3 Image reconstruction, root segmentation and analysis

177   The images were reconstructed using the commercial available Octopus 8.9 software

178   (Octopus, 2019), and images were corrected for neutron beam variation and camera noise

179   using the flat images and dark images taken before and after image acquisition (Dierick et al.,

180   2004; Vlassenbroeck et al., 2006). We did not use an scattering correction when processing

181   our images. The final reconstructed stack of images were imported into Avizo ® 9.0.1 for

182   root segmentation and analysis (FEI, 2015).

183   We attempted to use automated root segmentation algorithms RooTrack (Mairhofer et al.,

184   2012) and Root1 (Flavel et al., 2017) but due to the great heterogeneity in water content both

185   the soil and within roots, these proved unreliable for our samples. To get the best results,

186   roots were manually segmented using the limited range paintbrush editor in the segmentation

187   module in Avizo software. The segmented roots obtained from this process were then used to

188   calculate root lengths, thickness, surface area and volume for each root scan. Segmentation of

189   the larger seminal roots was primarily done using automated thresholding techniques

190   available in Avizo as there was a clear attenuation contrast between the soil and these roots.

191 This was however not done universally throughout the whole root system as most of the

192 smaller lateral roots as well as some sections of the larger seminal roots had attenuation

193 values that poorly contrasted or were even lower than that of moist soil and aggregates

194 surrounding them as shown in Figure 2. Time consuming manual segmentation based on a

195 combination of localised differences in attenuation and the connectivity of circularly shaped

196 pixel groups (as roots are usually circular in shape) enabled the segmentation of the

197 outstanding lateral roots and seminal root sections throughout the soil columns. Calibration

198 for water content was done using the same soil used in our experiments with known

199 volumetric water contents similar to what was done in Moradi et al., (2011). We then used

200 this calibration to relate the relative neutron attenuation to the moisture content for all the

201 images we acquired.
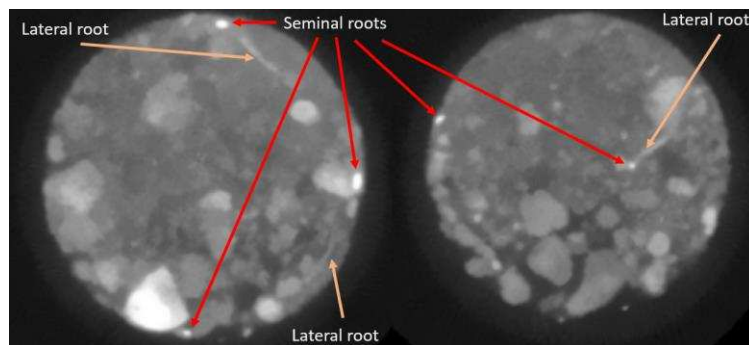
202

203 Figure 2: Grayscale images used to segment out roots showing how the different root types
204 contrasted with the soil.
205

206 2.4 WinRhizo® root analysis

207 As segmentation was a subjective process, we compared the root properties obtained from

208 our analysis with those obtained from flatbed scanning results analysed using WinRhizo ®

209 (Regents Instruments, Inc.). Therefore, after CT scanning, the soils columns were

210 destructively sampled and the soil was washed off from the roots over a 250μm sieve. The

211 washed roots were then placed in a specially designed water tray and scanned using an Epson

212 Expression 10000XL Pro at 600dpi resolution. This scan obtained 2D images of the plant

213 roots which were then analysed using WinRHIZO® 2016a software to determine the root

214 properties (Wang and Zhang, 2009). These roots alongside their shoots were then dried at

215 65°C for 48 hours to obtain their dry biomass.

216 2.5 Statistical analysis

217 All graphs and statistical analysis for these experiments was performed using GraphPad

218 Prism 8.0.1 (https://www.graphpad.com/) with a two tailed paired T tests used to separate

219 means.

220 **3. Results**

221 3.1 3D wheat root architecture from NCT

222 Three-dimensional root architectural properties of the 13-day old wheat seedlings rendered

223 from neutron scanning were successfully mapped with images in Fig 3. illustrating the

224 different root systems of the six plants that were grown.
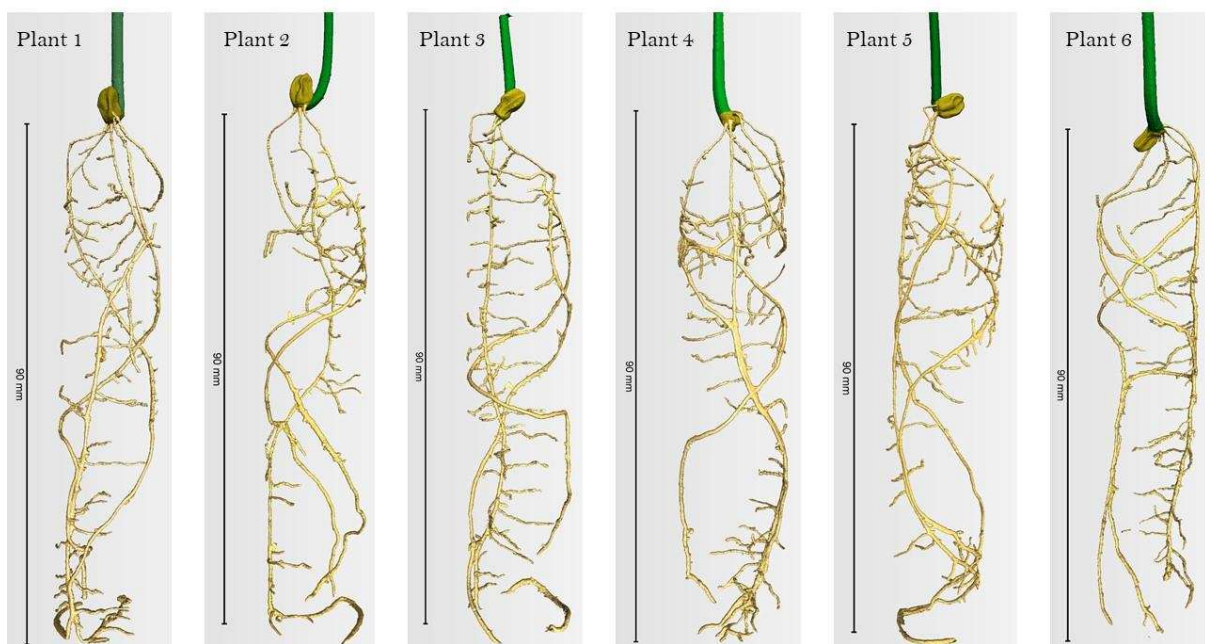
225

226 Figure 3: Images revealing the root architecture of the 6 different plants grown

10

227　The root architecture of the plants was broadly similar with an average total root length of

228　89.775 cm ±4.418 (SEM). The plants had 3-5 seminal roots at the time of imaging with least

229　one of the roots (mainly the primary root) having grown to reach to the base of the growth

230　tube they were growing in. Lateral roots of the different plants extended throughout the soil

231　column with visible differences in lateral root growth especially in regions where the seminal

232　roots were in close proximity to larger aggregates (1-4mm) that had large pores in-between

233　them. Lateral roots growing in these regions tended to be fewer and longer whilst those

234　growing in finer soil particles were more numerous but visibly shorter. This can be seen in

235　Figure 4 where due to the random segregation of particles when packing, larger aggregates

236　settled on one side of the column. Roots in some of the columns (plant 1, 4 and 6 in Figure 3)

237　also coalesced together and grew side by side in their downwards trajectory, only

238　disentangling lower down the soil column.
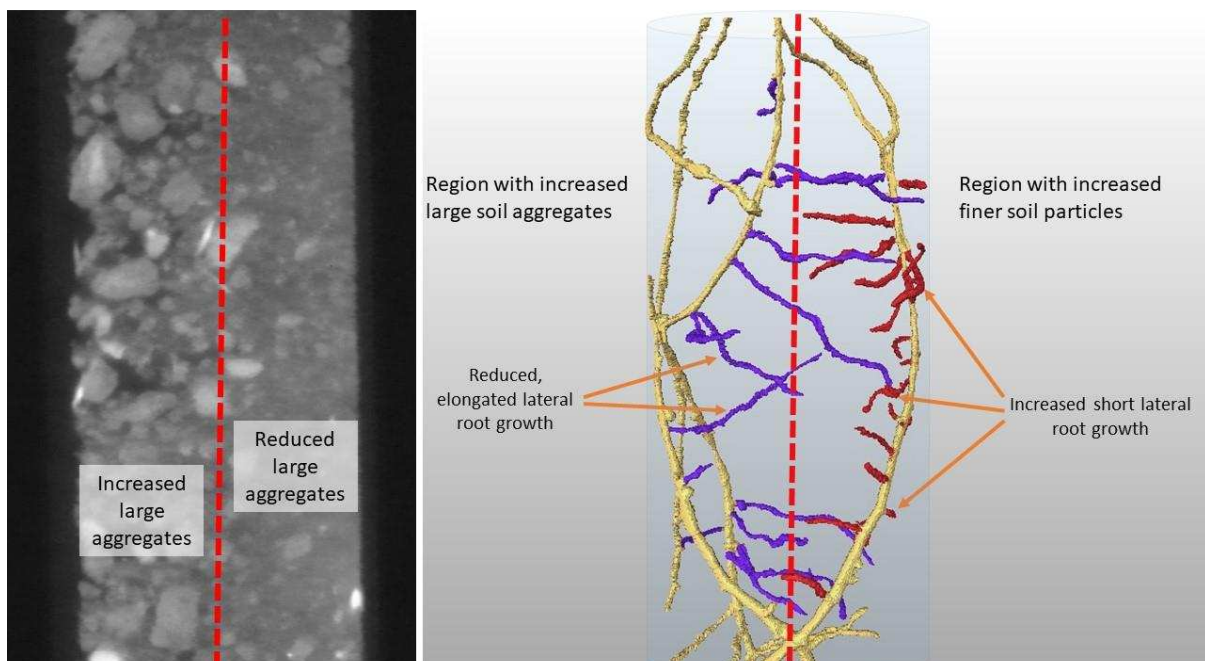
239

240　Figure 4 (Left)Greyscale image of a growth tube showing a segregation of large aggregates
241　towards the left side of growth tube. (Right) increased shorter lateral root growth in regions
242　with finer soil particles whilst lateral roots growing in regions with increased larger
243　aggregates are reduced and longer. The red line demarcates an arbitrary boundary between
244　regions dominated by large aggregates or finer particles. Longer lateral roots are shown in
245　purple whilst short lateral roots are shown in red.

246   3.2 Comparison between 3D and 2D root properties

247   Root properties calculated using WinRhizo ® from the flatbed scanning and 3D NCT enabled

248   the correlation of the two methods thus ensuring the validity of the method we used to

249   segment out the roots. Visual comparison between images obtained using the two methods as

250   shown in Figure 5 showed great similarities between them.
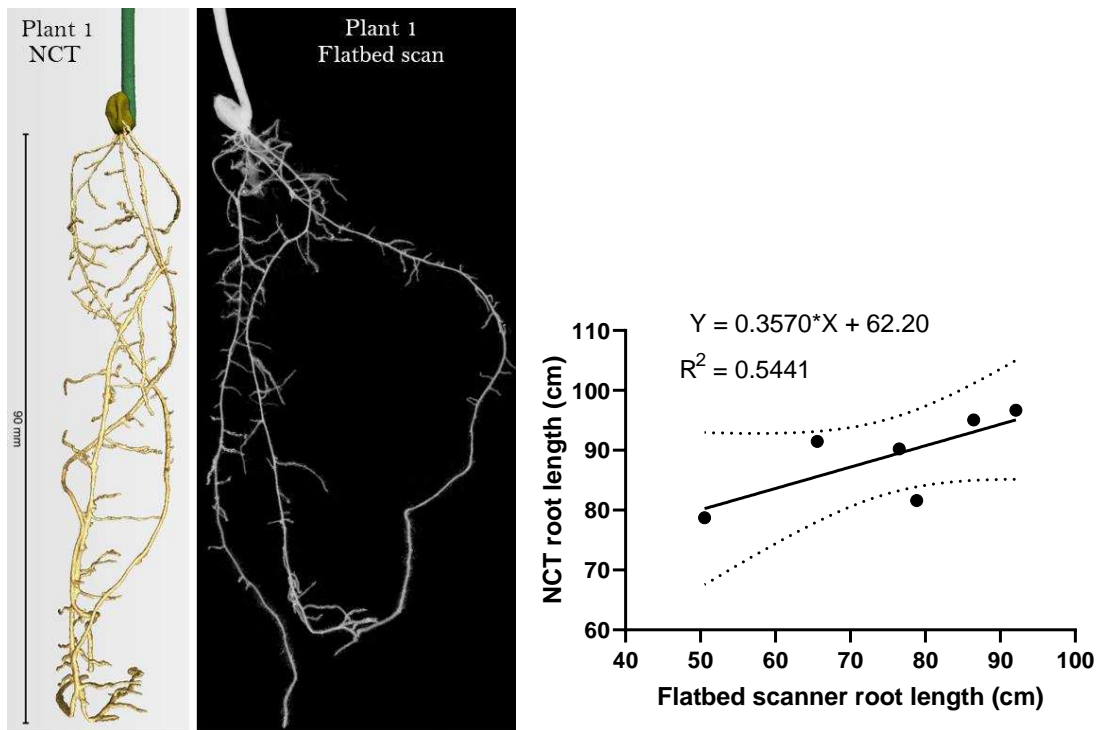
251

252   Figure 5: Side by side comparison of the same plant imaged using NCT and flatbed scanning
253

254   There was also a moderately strong linear relationship (R^2= 0.5441) between the root length

255   estimated by the two methods as given in Figure 5. As shown in Figure 6, estimates of root

256   length and surface area from neutron scans were significantly ($P<0.05$) higher than those

257   from flatbed scanning whilst root volume and thickness did not vary between the two

258   methods. The thinnest roots we could detect were around 110μm (2 voxels) in diameter

259   which corresponds to double our image pixel size according to Nyquist–Shannon theorem.
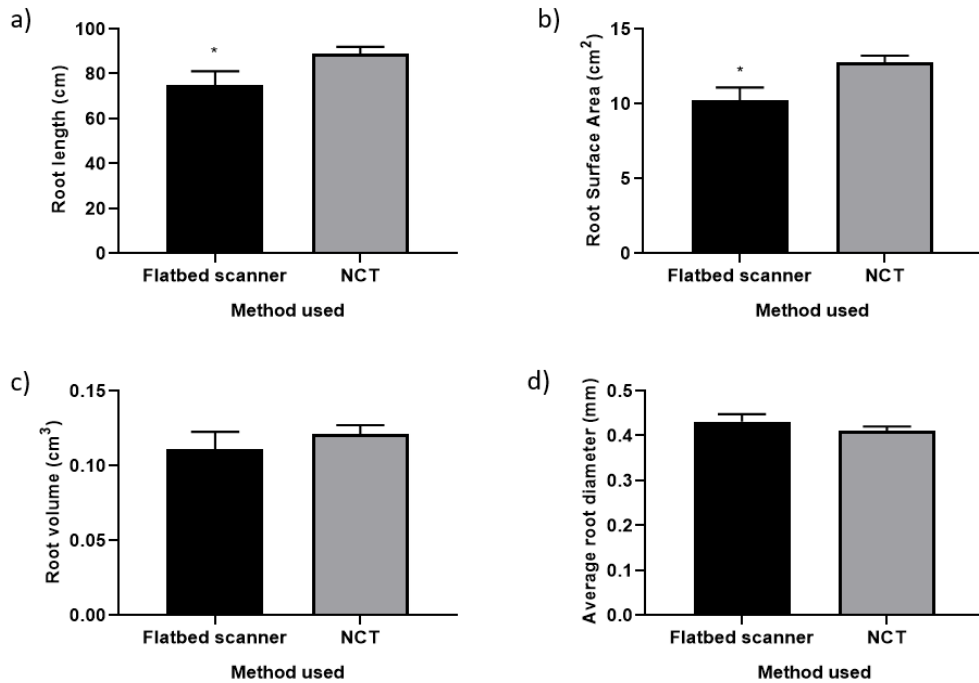
Figure 6: Comparison of root architectural properties as estimated by flatbed scanning and NCT. a) Root length (P= 0.0250), b) Root surface area, c) Root volume and d) Average root diameter. The error bars indicate Standard Error of the mean and * indicates significant differences (P< 0.05)

3.3 Soil moisture distribution

Similar to root architecture, the visualisation of soil moisture distribution was possible in 3D NCT as illustrated in Figure 7 with neutron attenuation being used as a proxy for θ using calibrated estimates of water content. These were calibrated by a series of scans of dry soil samples similar (but not identical) to those used for plant growth. It is worth noting however that our estimation of moisture content may encompass an add on effect with the high organic matter which increases neutron attenuation.

13

273
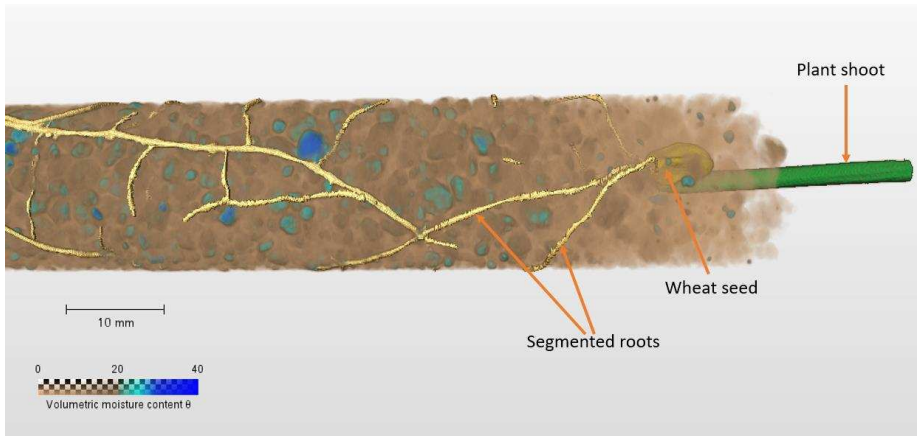
Figure 7: 3D NCT rendering of water distribution in aggregated soil where wheat seedling is growing

274
275

276

Water distribution within the columns was sporadic with regions of increased moisture

localisation and depletion throughout the different tubes. Water depletion was greatest in the

top 20mm of the soil with soil moisture gradually increasing between 20-60mm from the top

of the column until it reached its greatest extent at the base of the tube. Water was largely

localised in regions with nearly spherically shape regions within the soil as shown in Figure

8. Upon further analysis, it was discovered that this moisture accumulation was mainly

associated with the heterogeneously distributed soil aggregates within the soil. As compared

to finer particles, all or parts of aggregates have a $\theta > 20\%$.

285
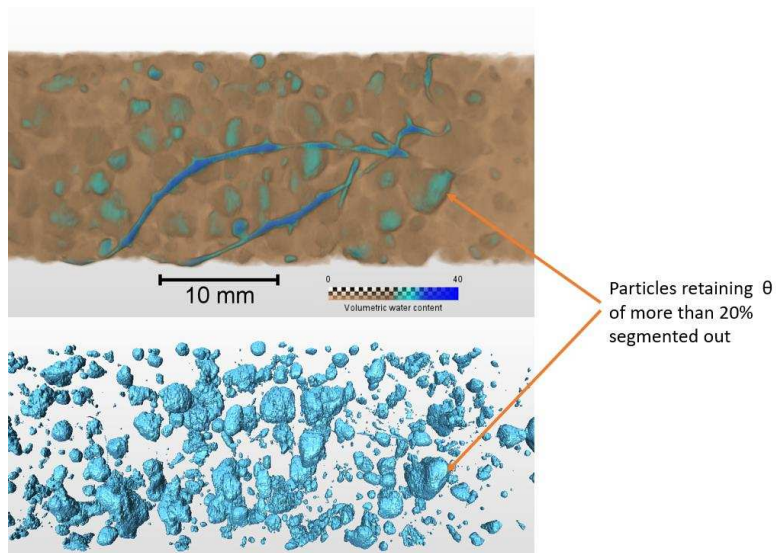
Figure 8: Showing segmenting out of particles retaining greater $\theta > 20\%$

286

14

287   3.4 Root interactions with soil moisture

288   Wheat roots did not preferentially grow in regions of increased θ (blue regions with $\theta >20$).

289   Many of the roots that were observed did not penetrate into water rich aggregates but rather

290   grew around them. Roots that were in direct contact with aggregates with a higher θ exhibited

291   an increase in their internal θ. In large pores in-between soil aggregates, roots had reduced θ

292   which was especially true in smaller lateral roots as opposed to the much larger seminal root

293   network. Some seminal roots however also showed this unexpected internal θ decrease when

294   growing through larger inter-aggregate pores. The rhizosphere around the roots as shown in

295   Figure 10, did not show great differences in θ as compared to the rest of the soil with

296   delineation of the extent of the rhizosphere being difficult decipher.
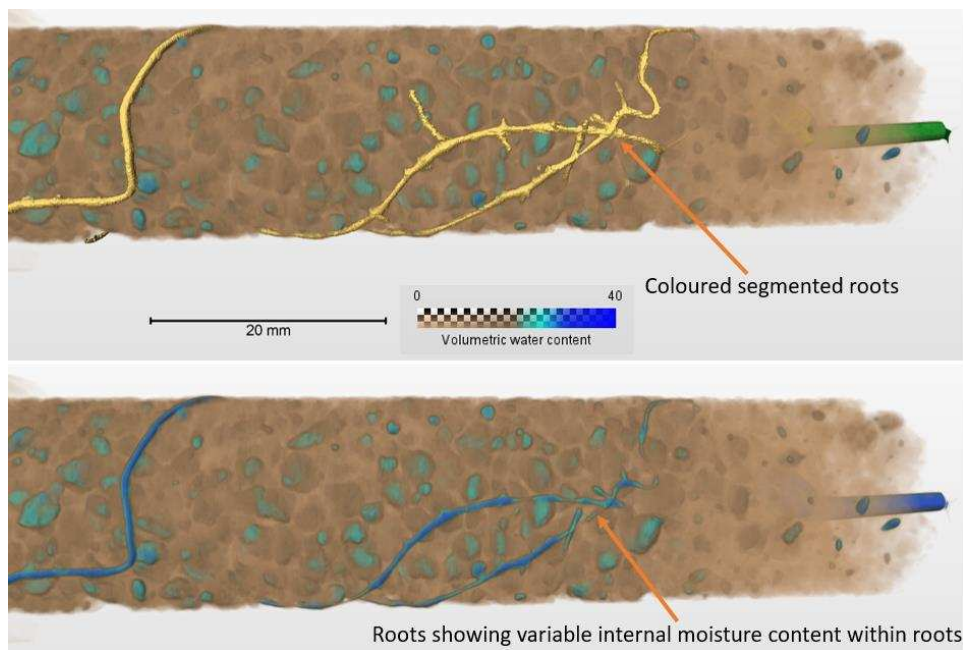
297

298   Figure 9: Variations in internal water content within roots growing through soil. The top
299   image shows segmented root indicated in yellow whilst in the bottom image, only root
300   moisture content can be visualised
301
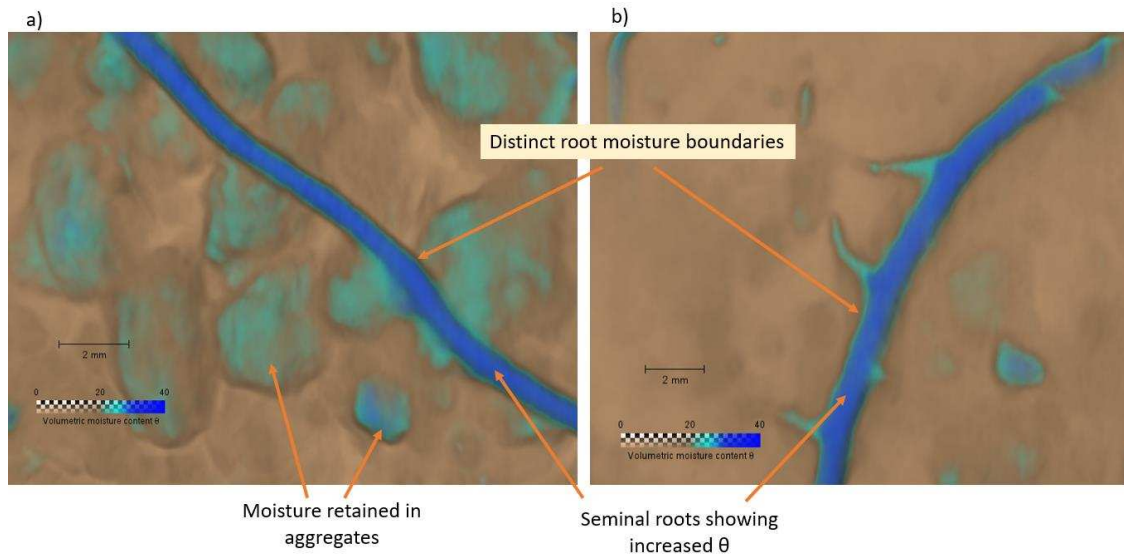
Figure 10: Close up view of the water-map in around seminal roots at a) 3cm and b) 5 cm below the soil surface showing distinct boundaries around the roots

4. Discussion

4.1 3D NCT wheat root architecture

The results presented show that detailed 3D root architectural properties of wheat growing in an aggregated soil with a moderately high organic matter content can successfully be visualised using NCT. To the best of our knowledge, this is the first study to use NCT to study root architectural development in wheat plants in detail. This research also represents a significant step away from many of the previous NCT root architectural studies such as those done by Nakanishi et al., (2005), Moradi et al., (2011), Warren et al., (2013) and Tötzke et al., (2017) that have used predominantly sand soils (with >90% sand). The sand soils used in the previously mentioned studies are more or less homogeneous and often lack aggregation. This study thereby seeks to break with convention by using a heterogeneous, aggregated soil with increased SOM. We recognise however, that the use of an aggregated soils as in this study presents a potential challenge when attempting to segment out wheat roots. This difficulty is brought about by the heterogeneity in soil properties with isolated regions retaining increased moisture and/or being high in organic matter (e.g. soil aggregates) that are

320   highly neutron attenuating due to their increased hydrogen content (Robinson, et al. 2008).

321   As a consequence of such features, there is a reduction in the clear attenuation difference

322   between the soil and plant root matter that is characteristic in sand soils thus complicating

323   segmentation as simple thresholding would yield inaccurate results. In this study we were

324   able to overcome such difficulty by both localised thresholding using the increased

325   attenuation and interconnectivity between roots as well as intuitive manual segmentation

326   techniques.

327   This study represents a move away from the use of the leguminous dicotyledonous plant

328   lupine (Lupinus albus. L) that has been popularly studied in many NCT and neutron

329   radiography experiments ever since the pioneering work of (Nakanishi, et al. 1992) and then

330   Menon et al., (2007) who established this plant as a 'model' for non-invasive neutron

331   imaging studies in plant-soil systems (Zarebanadkouki et al., 2012; Rudolph-Mohr, et al.

332   2014; Ahmed et al., 2017). Our use of the monocotyledonous graminae family plant, wheat

333   represents one of the first attempts at visualising the RSA of a staple food crop using NCT.

334   Many of the non-invasive imagery done on wheat plants has been carried out exclusively

335   using X-Ray CT (Flavel et al., 2014, 2012; Jenneson et al., 1999; Mooney et al., 2006; Tracy

336   et al., 2012). This study thereby demonstrates the feasibility of using NCT to study the RSA

337   of not only wheat plants but also other staple monocotyledonous crops such as rice and

338   maize.

339   4.2 Comparison between 3D and 2D root properties

340   As the manual segmentation methods we used to reveal root architecture from NCT scans

341   could be subjective, a comparison between the results obtained from NCT scanning and

342   flatbed scanner scanning was done. This is the first time results from NCT have been

343   compared to images flatbed scanning results. Similar correlations have previously been done

17

344   in on X-Ray CT scan root measurements such as those by Tracy et al., (2015) and Flavel et

345   al., (2012). In this study, here was moderately good correlation ($R^2 = 0.54$) between the two

346   methods with respect to key essential root characteristics, root length and volume with

347   estimates from flatbed scanning being significantly lower in root length. This could be

348   explained by the fact that some roots are inevitably lost during washing with literature

349   estimating a loss of about 20-40% of dry matter during storage and washing operations for

350   wheat roots (van Noordwijk and Floris, 1979; Grzebisz. et al, 1989). These losses though,

351   may be partially compensated for by the inability of our NCT to measure and quantify roots

352   less than 110 µm (55µm pixel size ×2) which is 2 times each voxel size that is widely

353   regarded as the effective spatial resolution limit of CT images (Moradi et al., 2011). Roots of

354   this thickness can be picked up by flatbed scanning provided they are not lost during the

355   washing process.

356   4.3 Soil moisture distribution

357   Similar to root system architecture, visualisation of soil moisture distribution was possible in

358   3D with the greyscale intensity acting as a proxy for θ. The high soil moisture heterogeneity

359   within the scanned tubes was as expected since soil heterogeneity often results in variable

360   hydraulic conductivity throughout the soil which has a direct bearing on the θ in unsaturated

361   conditions. As plants were surface irrigated, θ was lowest at the soil surface increasing

362   steadily towards the base of the growth tube. This accumulation of water at the base of the

363   tubes may have been brought about by the lack drainage as they were sealed at the base to

364   allow for accurate determination of the gravimetric water content. Localisation of water as

365   shown in Figure 8, which was presumed to be as a result to the preferential retention of water

366   in aggregates. This preferential water retention was presumed to arise from the pore size

367   distribution within soil aggregates which is often comprised of multiple micro-pores with the

368   ability to store water at higher suctions as opposed to the inter-aggregate pores referred to in

369   literature as structural pore spaces that are characteristically bigger and thus can freely

370   transmit water. This preferential water retention however was not universal as some

371   aggregates were also relatively dry at the time of imaging with some parts of the moist

372   aggregates also being relatively drier as compared to the rest of the aggregate. This may

373   suggest that that some aggregates may have pores large enough to drain freely at lower

374   suction levels.

375   Inference of soil moisture status using NCT and neutron radiography is not new with several

376   scholars having shown soil moisture distribution in sand soils. This study builds on their

377   findings adding further complexity by looking at an aggregated soil that has an increased

378   organic matter content. This introduces inaccuracies with the estimation of water content as

379   in such a soil, water is not the only highly neutron attenuating substance as organic matter has

380   increased hydrogen atom content as compared to soil (Robinson, et al. 2008; Tumlinson et

381   al., 2008). This thus means the total attenuation of each voxel is dependent on the water

382   content as well as the organic matter content for the particular volume of soil under review.

383   In this study we calibrated for water content using the same soil at varying levels of θ,

384   however in doing this we assumed that the organic matter content throughout the soil was

385   constant and variation in attenuation was primarily due to increased soil moisture content.

386   This estimation would be inaccurate especially in regions with localised elevated level of soil

387   organic matter. As such our interpretation of soil moisture distribution should be taken with

388   this in consideration.

389   4.4 Root interactions with soil moisture

390   As roots did not seem to grow preferentially in regions of relative high θ (are not highly

391   hydrotropic), it is clear that many other factors such as gravity, pore size distribution and

392   nutrient status of the soil may have also contributed to root growth patterns (Kar, et al. 1979;

19

393   Niu et al., 2015; Sato et al., 2015). As roots grew around different aggregates probably as a

394   consequence of trying to find the path of least resistance, many of the roots had good contact

395   with the surface of the moist aggregates. Roots in contact with moist aggregate surfaces

396   seemed to be able to extract water from these aggregates as more often than not, these roots

397   exhibited an increased in θ. It was striking however that roots growing though large air

398   spaces within the soil in some cases seemed to exhibit a reduction in θ as they passed through

399   the pore space. This is thought to be as a result of increased evaporative water loss from the

400   root surface within these large air spaces. Such large inter-aggregate pores may thus act as a

401   hindrance to internal root hydraulic conductivity and thus limiting the functionality of roots

402   growing through them. This finding could in part explain some of the observations seen by

403   (Passioura and Stirzaker, 1993) as well as Alexander and Miller (1991) who noticed a

404   general reduction in plant growth when artificial holes are introduced or when plants are

405   grown soils with large aggregate sizes.

406   Another unexpected result from our study was the absence of a distinct region of increased θ

407   around the roots demarcating rhizosphere soil around the roots as shown in Figure 10. This is

408   contrary to what has been observed in many neutron studies such as those done by (Moradi et

409   al., 2011) who noticed this distinct feature in all the plants they studied. This variation could

410   be as a result of our use of a different textured soil that may not produce such distinct features

411   as soil moisture was heterogeneously distributed within the soil. Differences in plant species

412   difference i.e. wheat used in this study as compared to maize or lupins mainly used in

413   previous studies could also be a contributory factor to our observed differences. Another

414   plausible explanation for this could be in the difference of root segmentation protocols that

415   were used in the different studies. In this case where semi-automatic and manual

416   segmentation was employed based on the roots distinct increased attenuation properties, the

417   edges of the roots could be mistaken to lie within the rhizosphere. This is however unlikely as

418 the root thickness as estimated NCT compare well to that found by flatbed scanning.

419 Questions may also be asked about the demarcation of root boundaries in the previous studies

420 as many of these studies did not compare the thickness of the roots found in their scans to

421 those obtained by manual measurement.

422 **5. Conclusion**

423 NCT was found to be able to reveal root architecture of wheat plants grown in an aggregated

424 sandy loam soil with appreciable amounts of organic matter and inherent heterogeneity. This

425 marks a step forward from the use of predominantly sand soils in NCT, albeit with new

426 challenges of its own. Macro-aggregates increased water storage within the soil with their

427 heterogeneous distribution determining the water distribution patterns across the soil after a

428 period of drying which could help plants water acquisition in times of limited water supply.

429 Lateral root growth was found to be reduced in regions with increased macro aggregates with

430 roots growing through large inter-aggregate pores exhibiting loss of moisture that could

431 potentially limit root function. Our work highlights how soil heterogeneity may affect water

432 distribution and plant-soil interactions thus encouraging the further use of NCT technology to

433 answer questions related soil water distribution in heterogeneous media for better modelling

434 of soil water movement.

440 **Conflicts of Interest**

The authors declare no conflict of interest. The funders had no role in the design of the study; in the collection, analyses, or interpretation of data; in the writing of the manuscript, or in the decision to publish the results.

References

Ahmed, M.A., Zarebanadkouki, M., Ahmadi, K., Kroener, E., Kostka, S., Kaestner, A., Carminati, A., 2017. Engineering Rhizosphere Hydraulics: Pathways to Improve Plant Adaptation to Drought. Vadose Zo. J. 0, 0. https://doi.org/10.2136/vzj2016.09.0090

Ahmed, S., Klassen, T.N., Keyes, S., Daly, M., Jones, D.L., Mavrogordato, M., Sinclair, I., Roose, T., 2016. Imaging the interaction of roots and phosphate fertiliser granules using 4D X-ray tomography. Plant Soil 401, 125–134. https://doi.org/10.1007/s11104-015-2425-5

Alahmad, S., El Hassouni, K., Bassi, F.M., Dinglasan, E., Youssef, C., Quarry, G., Aksoy, A., Mazzucotelli, E., Juhász, A., Able, J.A., Christopher, J., Voss-Fels, K.P., Hickey, L.T., 2019. A Major Root Architecture QTL Responding to Water Limitation in Durum Wheat. Front. Plant Sci. 10, 436. https://doi.org/10.3389/fpls.2019.00436

Bačić, G., Ratković, S., 1987. NMR studies of radial exchange and distribution of water in maize roots: The relevance of modelling of exchange kinetics. J. Exp. Bot. 38, 1284–1297. https://doi.org/10.1093/jxb/38.8.1284

Blunk, S., Malik, A.H., de Heer, M.I., Ekblad, T., Bussell, J., Sparkes, D., Fredlund, K., Sturrock, C.J., Mooney, S.J., 2017. Quantification of seed-soil contact of sugar beet (Beta vulgaris) using X-ray Computed Tomography. Plant Methods 13, 1–14. https://doi.org/10.1186/s13007-017-0220-4

Bois, J.F., Couchat, P.H., 1983. Comparison of the Effects of Water Stress on the Root

Systems of Two Cultivars of Upland Rice (Oryza satíva L .). Ann. Bot. 52, 479–487.

Borlaug, N., Dowswell, C., 2003. Feeding a world of ten billion people: a 21st century challenge. … Int. Congr. Wake … 3–23.

Brown, D.P., Pratum, T.K., Bledsoe, C., Ford, E.D., Cothern, J.S., Perry, D., 1991. Noninvasive studies of conifer roots: nuclear magnetic resonance (NMR) imaging of Douglas-fir seedlings. Can. J. For. Res. 21, 1559–1566.

Burca, G., Kockelmann, W., James, J.A., Fitzpatrick, M.E., 2013. Modelling of an imaging beamline at the ISIS pulsed neutron source. J. Instrum. 8. https://doi.org/10.1088/1748-0221/8/10/P10001

Burca, G., Nagella, S., Clark, T., Tasev, D., Rahman, I.A., Garwood, R.J., Spencer, A.R.T., Turner, M.J., Kelleher, J.F., 2018. Exploring the potential of neutron imaging for life sciences on IMAT. J. Microsc. 00, 1–6. https://doi.org/10.1111/jmi.12761

Burr-Hersey, J.E., Mooney, S.J., Bengough, A.G., Mairhofer, S., Ritz, K., 2017. Developmental morphology of cover crop species exhibit contrasting behaviour to changes in soil bulk density, revealed by X-ray computed tomography. PLoS One 12, 1–18. https://doi.org/10.1371/journal.pone.0181872

Carminati, A., Moradi, A.B., Vetterlein, D., Vontobel, P., Lehmann, E., Weller, U., Vogel, H.J., Oswald, S.E., 2010. Dynamics of soil water content in the rhizosphere. Plant Soil. https://doi.org/10.1007/s11104-010-0283-8

Cassman, K.G., 1999. Ecological intensification of cereal production systems: yield potential, soil quality, and precision agriculture. Proc. Natl. Acad. Sci. U. S. A. 96, 5952–9. https://doi.org/10.1073/pnas.96.11.5952

Couchat, P., Moutonnet, P., Houelle, M., Picard, D., 1980. In situ study of corn seedling root

487   and shoot growth by neutron radiography. Agron. J. 72, 321-324 ST-In situ study of

488   corn seedling root.

489 Crestana, S., Cesareo, R., Mascarenhas, S., 1986. Using a computed tomography miniscanner

490   in soil science. Soil Sci. 142, 56–61.

491 Dierick, M., Masschaele, B., Van Hoorebeke, L., 2004. Octopus, a fast and user-friendly

492   tomographic reconstruction package developed in LabView. Meas. Sci. Technol. 15,

493   1366–1370. https://doi.org/10.1088/0957-0233/15/7/020

494 Esser, H.G., Carminati, A., Vontobel, P., Lehmann, E.H., Oswald, S.E., 2010. Neutron

495   radiography and tomography of water distribution in the root zone. J. Plant Nutr. Soil

496   Sci. 173, 757–764. https://doi.org/10.1002/jpln.200900188

497 FAOSTAT, 2019. FAOSTAT database [WWW Document]. Food Agric. Organ. United

498   Nations, Rome, Italy. URL http://www.fao.org/faostat/en/#home

499 FEI, 2015. User's guide Avizo ® 9 [WWW Document].

500 Figueroa-Bustos, V., Palta, J., Chen, Y., Siddique, K., 2018. Characterization of Root and

501   Shoot Traits in Wheat Cultivars with Putative Differences in Root System Size.

502   Agronomy. https://doi.org/10.3390/agronomy8070109

503 Flavel, R.J., Guppy, C.N., Rabbi, S.M.R., Young, I.M., 2017. An image processing and

504   analysis tool for identifying and analysing complex plant root systems in 3D soil using

505   non-destructive analysis : Root1 1–18. https://doi.org/10.7910/DVN/DXG4AH.Funding

506 Flavel, R.J., Guppy, C.N., Tighe, M., Watt, M., McNeill, A., Young, I.M., 2012. Non-

507   destructive quantification of cereal roots in soil using high-resolution X-ray tomography.

508   J. Exp. Bot. 63, 2503–2511. https://doi.org/10.1093/jxb/err421

509 Flavel, R.J., Guppy, C.N., Tighe, M.K., Watt, M., Young, I.M., 2014. Quantifying the

510   response of wheat (Triticum aestivum L) root system architecture to phosphorus in an

511   Oxisol. Plant Soil 385, 303–310. https://doi.org/10.1007/s11104-014-2191-9

512   Furukawa, J., Nakanishi, T.M., Matsubayashi, M., 1999. Neutron radiography of a root

513   growing in soil with vanadium. Nucl. Instruments Methods Phys. Res. Sect. A Accel.

514   Spectrometers, Detect. Assoc. Equip. 424, 116–121. https://doi.org/10.1016/S0168-

515   9002(98)01279-0

516   Gewin, V., 2010. An underground revolution. Nature 466, 522–533.

517   Grzebisz, W., Floris, W., van Noordwijk, M., 1989. Loss of dry matter and cell contents from

518   fibrous roots of sugar beet due to sampling , storage and washing * 57, 53–57.

519   IPCC, 2007. Climate Change 2007: The Physical Science Basis, in: Solomon, S.D., Qin, M.,

520   Manning, M., Chen, Z., Marquis, M., Averyt, K.B., Tignor, M., Miller, H.L. (Eds.),

521   Contribution of Working Group I to the Fourth Assess- Ment Report of the

522   Intergovernmental Panel on Climate Change. Cambridge,UK and New York, USA.

523   Jenneson, P.M., Gilboy, W.B., Morton, E.J., Luggar, R.D., Gregory, P.J., 1999. Optimisation

524   of X-ray micro-tomography, in: 1999 IEEE Nuclear Science Symposium. Conference

525   Record. 1999 Nuclear Science Symposium and Medical Imaging Conference (Cat.

526   No.99CH37019).

527   Kar, S., Varade, S.B., Ghildyal, B.P., 1979. Pore size distribution and root growth relations of

528   rice in artificially synthesized soils. Soil Sci. https://doi.org/10.1097/00010694-

529   197912000-00008

530   Keyes, S.D., Daly, K.R., Gostling, N.J., Jones, D.L., Talboys, P., Pinzer, B.R., Boardman, R.,

531   Sinclair, I., Marchant, A., Roose, T., 2013. High resolution synchrotron imaging of

532   wheat root hairs growing in soil and image based modelling of phosphate uptake. New

533 Phytol. 198, 1023–1029. https://doi.org/10.1111/nph.12294

534 Khoury, C.K., Bjorkman, A.D., Dempewolf, H., Ramirez-Villegas, J., Guarino, L., Jarvis, A.,

535 Rieseberg, L.H., Struik, P.C., 2014. Increasing homogeneity in global food supplies and

536 the implications for food security. Proc. Natl. Acad. Sci. U. S. A. 111, 4001–6.

537 https://doi.org/10.1073/pnas.1313490111

538 Knox, J., Hess, T., Daccache, A., Wheeler, T., 2012. Climate change impacts on crop

539 productivity in Africa and South Asia. Environ. Res. Lett. 7, 34032.

540 https://doi.org/10.1088/1748-9326/7/3/034032

541 Kockelmann, W., Zhang, S.Y., Kelleher, J.F., Nightingale, J.B., Burca, G., James, J.A., 2013.

542 IMAT - A new imaging and diffraction instrument at ISIS. Phys. Procedia 43, 100–110.

543 https://doi.org/10.1016/j.phpro.2013.03.013

544 Koebernick, N., Daly, K.R., Keyes, S.D., George, T.S., Brown, L.K., Raffan, A., Cooper,

545 L.J., Naveed, M., Bengough, A.G., Sinclair, I., Hallett, P.D., Roose, T., 2017. High-

546 resolution synchrotron imaging shows that root hairs influence rhizosphere soil structure

547 formation. New Phytol. https://doi.org/10.1111/nph.14705

548 Lal, R., 2016. Feeding 11 billion on 0.5 billion hectare of area under cereal crops.

549 https://doi.org/10.1002/fes3.99

550 Lynch, J.P., 2007. Roots of the second green revolution. Aust. J. Bot. 55, 493–512.

551 https://doi.org/10.1071/BT06118

552 Mairhofer, S., Zappala, S., Tracy, S.R., Sturrock, C., Bennett, M., Mooney, S.J., Pridmore,

553 T., 2012. RooTrak: Automated Recovery of Three-Dimensional Plant Root Architecture

554 in Soil from X-Ray Microcomputed Tomography Images Using Visual Tracking. Plant

555 Physiol. 158, 561–569. https://doi.org/10.1104/pp.111.186221

556 Mawodza, T., Brooks, H., Burca, G., Menon, M., 2018. Understanding root architecture and

557   water uptake of water use efficient wheat mutants using neutron and X-Ray CT imaging.

558   STFC ISIS Neutron Muon Source Data J.

559 Menon, M., Robinson, B., Oswald, S.E., Kaestner, A., Abbaspour, K.C., Lehmann, E.,

560   Schulin, R., 2007. Visualization of root growth in heterogeneously contaminated soil

561   using neutron radiography. Eur. J. Soil Sci. 58, 802–810. https://doi.org/10.1111/j.1365-

562   2389.2006.00870.x

563 Metzner, R., Eggert, A., van Dusschoten, D., Pflugfelder, D., Gerth, S., Schurr, U., Uhlmann,

564   N., Jahnke, S., 2015. Direct comparison of MRI and X-ray CT technologies for 3D

565   imaging of root systems in soil: potential and challenges for root trait quantification.

566   Plant Methods. https://doi.org/10.1186/s13007-015-0060-z

567 Mooney, S.J., Morris, C., Berry, P.M., 2006. Visualization and quantification of the effects of

568   cereal root lodging on three-dimensional soil macrostructure using x-ray computed

569   tomography. Soil Sci. 171, 706–718.

570   https://doi.org/10.1097/01.ss.0000228041.03142.d3

571 Mooney, S.J., Pridmore, T.P., Helliwell, J., Bennett, M.J., 2012. Developing X-ray computed

572   tomography to non-invasively image 3-D root systems architecture in soil. Plant Soil

573   352, 1–22. https://doi.org/10.1007/s11104-011-1039-9

574 Moradi, A.B., Carminati, A., Vetterlein, D., Vontobel, P., Lehmann, E., Weller, U.,

575   Hopmans, J.W., Vogel, H.-J., Oswald, S.E., 2011. Three-dimensional visualization and

576   quantification of water content in the rhizosphere. New Phytol. 192, 653–663.

577   https://doi.org/10.1111/j.1469-8137.2011.03826.x

578 Moradi, A.B., Conesa, H.M., Robinson, B., Lehmann, E., Kuehne, G., Kaestner, A., Oswald,

579   S., Schulin, R., 2009. Neutron radiography as a tool for revealing root development in

580   soil: Capabilities and limitations. Plant Soil 318, 243–255.

581   https://doi.org/10.1007/s11104-008-9834-7

582 Nakanishi, T.M., Matsumoto, S., Kobayashi, H., 1992. Morphological Change of Plant Root

583   Revealed Radiography by Neutron of Tokyo 641, 638–641.

584 Nakanishi, T.M., Okuni, Y., Hayashi, Y., Nishiyama, H., 2005. Water gradient profiles at

585   bean plant roots determined by neutron beam analysis. J. Radioanal. Nucl. Chem. 264,

586   313–317. https://doi.org/10.1007/s10967-005-0713-x

587 Niu, Y., Jin, G., Li, X., Tang, C., Zhang, Y., Liang, Y., Yu, J., 2015. Phosphorus and

588   magnesium interactively modulate the elongation and directional growth of primary

589   roots in Arabidopsis thaliana (L .) Heynh 66, 3841–3854.

590   https://doi.org/10.1093/jxb/erv181

591 Octopus, 2019. Octopus reconstrsuction [WWW Document]. URL

592   https://octopusimaging.eu/octopus/octopus-reconstruction (accessed 3.1.19).

593 Oswald, S.E., Menon, M., Carminati, A., Vontobel, P., Lehmann, E., Schulin, R., 2008.

594   Quantitative Imaging of Infiltration, Root Growth, and Root Water Uptake via Neutron

595   Radiography. Vadose Zo. J. 7, 1035. https://doi.org/10.2136/vzj2007.0156

596 Passioura, J.B., Stirzaker, R.J., 1993. Feedforward Responses of Plants to Physically

597   Inhospitable Soil. Int. Crop Sci. I 715–719.

598   https://doi.org/10.2135/1993.internationalcropscience.c114

599 Pflugfelder, D., Metzner, R., Dusschoten, D. Van, Reichel, R., Jahnke, S., Koller, R., 2017.

600   Non-invasive imaging of plant roots in different soils using magnetic resonance imaging

601   (MRI). Plant Methods 1–9. https://doi.org/10.1186/s13007-017-0252-9

602 Pierret, A., Moran, C.J., Doussan, C., 2005. Conventional detection methodology is limiting

our ability to understand the roles and functions of fine roots. New Phytol. 166, 967–

980. https://doi.org/10.1111/j.1469-8137.2005.01389.x

Rich, S.M., Watt, M., 2013. Soil conditions and cereal root system architecture: Review and

considerations for linking Darwin and Weaver. J. Exp. Bot. 64, 1193–1208.

https://doi.org/10.1093/jxb/ert043

Robinson, B.H., Moradi, A., Lehmann, E., 2008. Neutron Radiography for the Analysis of

Plant – Soil Interactions. Encycl. Anal. Chem. Appl. Theory Instrum. 1–8.

Rudolph-Mohr, N., Vontobel, P., Oswald, S.E., 2014. A multi-imaging approach to study the

root-soil interface. Ann. Bot. 114, 1779–1787. https://doi.org/10.1093/aob/mcu200

Sato, E.M., Hijazi, H., Bennett, M.J., Vissenberg, K., Swarup, R., 2015. New insights into

root gravitropic signalling. J. Exp. Bot. 66, 2155–2165.

https://doi.org/10.1093/jxb/eru515

Senapati, N., Semenov, M.A., 2019. Assessing yield gap in high productive countries by

designing wheat ideotypes. Sci. Rep. 9, 5516. https://doi.org/10.1038/s41598-019-

40981-0

Southon, T.E., Mattsson, A., Jones, R.A., 1992. NMR imaging of roots: effects after root

freezing of containerised conifer seedlings. Physiol. Plant. 329–334.

Stingaciu, L., Schulz, H., Pohlmeier, A., Behnke, S., Zilken, H., Javaux, M., Vereecken, H.,

2013. In Situ Root System Architecture Extraction from Magnetic Resonance Imaging

for Water Uptake Modeling. Vadose Zo. J. 0, 0. https://doi.org/10.2136/vzj2012.0019

Tötzke, C., Kardjilov, N., Manke, I., Oswald, S.E., 2017. Capturing 3D Water Flow in

Rooted Soil by Ultra-fast Neutron Tomography. Sci. Rep. 7, 6192.

https://doi.org/10.1038/s41598-017-06046-w

626 Tracy, S.R., Black, C.R., Roberts, J.A., Dodd, I.C., Mooney, S.J., 2015. Using X-ray

627   Computed Tomography to explore the role of abscisic acid in moderating the impact of

628   soil compaction on root system architecture. Environ. Exp. Bot. 110, 11–18.

629   https://doi.org/10.1016/j.envexpbot.2014.09.003

630 Tracy, S.R., Black, C.R., Roberts, J.A., McNeill, A., Davidson, R., Tester, M., Samec, M.,

631   Korošak, D., Sturrock, C., Mooney, S.J., 2012. Quantifying the effect of soil compaction

632   on three varieties of wheat (Triticum aestivum L.) using X-ray Micro Computed

633   Tomography (CT). Plant Soil 353, 195–208. https://doi.org/10.1007/s11104-011-1022-5

634 Tracy, S.R., Black, C.R., Roberts, J.A., Mooney, S.J., 2013. Exploring the interacting effect

635   of soil texture and bulk density on root system development in tomato (Solanum

636   lycopersicum L.). Environ. Exp. Bot. 91, 38–47.

637   https://doi.org/10.1016/j.envexpbot.2013.03.003

638 Tumlinson, L.G., Liu, H., Silk, W.K., Hopmans, J.W., 2008. Thermal Neutron Computed

639   Tomography of Soil Water and Plant Roots. Soil Sci. Soc. Am. J. 72, 1234.

640   https://doi.org/10.2136/sssaj2007.0302

641 van Noordwijk, M., Floris, J., 1979. Loss of dry weight during washing and storage of root

642   samples. Plant Soil 53, 239–240.

643 Vlassenbroeck, J., Masschaele, B., Cnudde, V., Dierick, M., Pieters, K., Van Hoorebeke, L.,

644   Jacobs, P., 2006. Octopus 8: A High Performance Tomographic Reconstruction Package

645   for X-ray Tube and Synchrotron micro-CT, in: Advances in X-Ray Tomography for

646   Geomaterials. ISTE, London, UK, pp. 167–173.

647   https://doi.org/10.1002/9780470612187.ch13

648 Waines, J.G., Ehdaie, B., 2007. Domestication and crop physiology: roots of green-revolution

649   wheat. Ann. Bot. 100, 991–8. https://doi.org/10.1093/aob/mcm180

650   Wang, M. Ben, Zhang, Q., 2009. Issues in using the WinRHIZO system to determine

651   physical characteristics of plant fine roots. Shengtai Xuebao/ Acta Ecol. Sin. 29, 136–

652   138. https://doi.org/10.1016/j.chnaes.2009.05.007

653   Warren, J.M., Bilheux, H., Kang, M., Voisin, S., Cheng, C.L., Horita, J., Perfect, E., 2013.

654   Neutron imaging reveals internal plant water dynamics. Plant Soil 366, 683–693.

655   https://doi.org/10.1007/s11104-012-1579-7

656   Willatt, S.T., Struss, R.G., 1979. Germination and Early Growth of Plants using neutron

657   radiography 415–422.

658   Willatt, S.T., Struss, R.G., Taylor, H.M., 1978. In situ Root Studies Using Neutron

659   Radiography 1–6.

660   Zarebanadkouki, M., Carminati, A., Kaestner, A., Mannes, D., Morgano, M., Peetermans, S.,

661   Lehmann, E., Trtik, P., 2015. On-the-fly Neutron Tomography of Water Transport into

662   Lupine Roots, in: Physics Procedia. https://doi.org/10.1016/j.phpro.2015.07.041

663   Zarebanadkouki, M., Kim, Y.X., Carminati, A., 2013. Where do roots take up water? Neutron

664   radiography of water flow into the roots of transpiring plants growing in soil. New

665   Phytol. 199, 1034–1044. https://doi.org/10.1111/nph.12330

666   Zarebanadkouki, M., Kim, Y.X., Moradi, A.B., Vogel, H.-J., Kaestner, A., Carminati, A.,

667   2012. Quantification and Modeling of Local Root Water Uptake Using Neutron

668   Radiography and Deuterated Water. Vadose Zo. J. 11.

669   https://doi.org/10.2136/vzj2011.0196

670